Biol. Cybern. 83, 341–353 (2000)

Biological Cybernetics

Synchronous oscillation in the cerebral cortex and object coherence: simulation of basic electrophysiological findings

J. J. Wright, P. D. Bourke, C. L. Chapman

Mental Health Research Institute of Victoria, 155 Oak Street, Parkville, Melbourne, Victoria 3052, Australia

Received: 22 December 1998 / Accepted in revised form: 16 March 2000

Abstract. A lumped continuum model for electrocortical activity was used to simulate several established experimental findings of synchronous oscillation which have not all been previously embodied in a single explanatory model. Moving-bar visual stimuli of different extension, stimuli moving in different directions, the impact of non-specific cortical activation upon synchronous oscillation, and the frequency content of EEG associated with synchrony were considered. The magnitude of zero lag synchrony was primarily accounted for by the properties of the eigenmodes of the travelling local field potential superposition waves generated by inputs to the cortex, largely independent of the oscillation properties and associated spectral content. Approximation of the differences in cross-correlation observed with differently moving bar stimuli, and of the impact of cortical activation, required added assumptions on (a) spatial coherence of afferent volleys arising from parts of a single stimulus object and (b) the presence of low-amplitude diffuse field noise, with enhancement of cortical signal/noise ratio with respect to the spatially coherent inputs, at higher levels of cortical activation. Synchrony appears to be a ubiquitous property of cortex-like delay networks. Precision in the modelling of synchronous oscillation findings will require detailed description of input pathways, cortical connectivity, cortical stability, and aspects of cortical/subcortical interactions.

1 Introduction

Discovery of the phenomenon of synchronous oscillation in the cerebral cortex (e.g. Eckhorn et al. 1988; Gray et al. 1989; Singer 1994; Singer and Gray 1995) was partly motivated by a proposal by von der Malsburg (1983) that patterns of synchronous activity in the brain would offer a mechanism whereby the many sensory input features contributing to the perception of a unified object might be linked to form a whole. This offered a solution to the binding problem posed by the need to register unique combinations of all possible stimulus features (Singer and Gray 1995; Livingstone 1996).

As has been pointed out by Palm and Wennekers (1997), interest in this solution to the binding problem, rather than the simpler requirements of direct modelling of experimental results, has driven much of the attempts to find an explanatory mechanism for synchronous oscillation. A strong presumption that linked non-linear oscillations underlie the phenomenon (e.g. Abarbanel et al. 1996) has motivated most attempts at modelling the phenomenon. Yet there is little evidence that phase-locking of non-linear oscillators is necessarily involved (Wennekers and Palm 1997), considering the broad spectral band over which synchrony has been found (Bressler et al. 1993).

The significance of the experimental data now published on synchronous oscillation is very substantial, but remains controversial. Theoretical opinions vary from the view that synchrony may be essentially irrelevant to synaptic interactions (Amit 1998) to the possibility that synchrony is vital to the co-ordination of synaptic modifications in the brain (Phillips and Singer 1997). Experimental conditions leave a number of variables (connectivities, signal/noise ratios, etc.) unspecified. Meantime, attempts to model the process must be selective. Some experimental aspects of synchronous oscillation appear reasonably clearly defined.

Firstly, it is known that synchrony is most often observed in association with oscillation in the gamma band (e.g. Eckhorn 1988) but not uniquely so (Bressler et al. 1993).

Secondly, it appears that synchrony is strongest between cortical sites in which neurones seem to be involved in co-processing of sensory input, e.g. between columns of cells with similar orientation preference (Gray and Singer 1989; Livingstone 1996).

Correspondence to: J. J. Wright
(e-mail: jjw@mhri.edu.au; Fax: +61-393-875061)

Thirdly, it appears that increased cortical activation, such as is produced by driving the mesencephalic reticular formation, enhances synchronous oscillation (Munk et al. 1996).

Fourthly, properties of the stimulus object(s) play a part. One large bar moving across the visual field produces stronger synchrony than two small bars concurrently stimulating each of the relevant points in the retina, and bars moving in separate directions generally produce less synchrony than the same bars moving in the same direction across the visual field (Livingstone 1996; Neuenschwander and Singer 1996).

To attempt to provide a concise account for these experimental properties, we used a lumped continuum model of the cortex which provides an account of the general spectral content of EEG (Wright 1999). This approach is intended to complement other simulations which approximate physiological realism using feedforward networks with inhibitory surrounds, or single and multiple orientation domains (Schillen and Konig 1994; Fuentes et al. 1996; Xing and Gerstein 1996; Juergens and Eckhorn 1997). Our object was to ascertain the minimal assumptions needed to reproduce the experimental data. The model's parameterisation is as of yet approximate, and physiological detail is incomplete, but these limitations are not relevant to the demonstrations we will report. Models closely related to that applied here have been analysed with regard to cross-correlation properties under the condition that two points on the cortical surface are driven by independent white noise (Wright 1997; Chapman et al., in press; Robinson et al. 1998), yielding results which have guided the experimental design used here. In this model, synchrony depends wholly upon relatively long-range excitatory connections in a continuum field – dendritic lag-summations and relatively rapid axonal transmission being the essential ingredients – while short-range excitatory/inhibitory interactions appear crucial only to the occurrence of oscillation. These characteristics are very similar to those observed in neural network models with intracortical couplings only, observed by Wilson and Bower (1991). The continuum formulation supplements the neural network approach, by enabling a different insight into the physical nature of synchrony, since the essential non-linearity of individual elements is avoided, and the stochastic and essentially linear properties of the neuronal mass is emphasized. Likewise, these intracortical two-dimensional models contrast with the work of Lumer et al. (1997a,b), who studied conditions for synchrony and oscillation in a neural-network model of the thalamocortical system. They observed synchrony at many levels, which they attributed largely to re-entrant activity at multiple levels in the pathway.

In the present model, reproduction of the physiological experiments required additional simple assumptions about the signal-to-noise ratio of the cortex, and cross-correlation in afferent volleys associated with individual stimulus objects, as will be described with Sect. 2.

2 Methods

The simulation used here has been reported in Wright (1999). Parameters were chosen to accord with the following assumptions about the overall neuronal population properties:

1. Most synapses are located on the distal dendritic tree, so mean delay from synapses to soma is near the upper limit of physiological estimates for dendritic delay (Segev 1995; Thomson 1996, 1997).
2. Dendritic delays in excitatory and inhibitory cells, and from excitatory and inhibitory synapses, are comparable to first approximation.
3. Axonal delays are range dependent, but are always small compared to dendritic delays.
4. There is a finite probability that an action potential may be emitted by a given neurone, even at membrane potentials very close to the inhibitory reversal potential.
5. Synaptic gains are in the ratio of 4:1 for inhibitory synapses versus excitatory synapses (Segev 1995) and produce a high signal amplification (Thomson 1997) so that the stable operating range of cortical activity is restricted to low pulse densities.

2.1 State equations

The N cells in a unit volume each have a probability of emission of an action potential q_i as a function of their membrane potentials. The sum of population membrane potentials is taken to be directly proportional to the local field potential (LFP), $V(t)$ at time t. Then, in a mean-field approximation, the pulse-probability density $Q(t)$ is given by

$$Q = \frac{1}{N}\sum_{i=1}^{N} q_i(V) \quad . \tag{1}$$

By the central limit theorem, for large N, Q will have a Gaussian distribution with respect to V, whatever the individual distributions of q_i, so V and Q are approximately related by

$$Q = (1 + e^{a(V-3)})^{-1} \quad . \tag{2}$$

This sigmoidal relation is used to approximate the sigmoidal error function implied by the Gaussian population pulse probability distribution. Where $a = -\pi/\sqrt{3}$, LFP voltage units (vu) are approximate to standard deviations of the distribution of cell pulse probability over the complete range of LFP, with a 50% mean probability of pulse emission 3SD from complete polarisation of the neural population. Thus, Q has a value close to zero when $V = 0$, and approaching an asymptote of maximum pulse rate at $V = 6$ vu.

The time response of mean membrane potential (and by implication LFP and soma potential) is given by

$$V(t) = g\sum_{j=1}^{n} w_j Q_a(t - j\Delta t), \quad j = 1, 2, 3 \ldots n \quad , \tag{3}$$

where g is synaptic gain, Q_a is afferent pulse action density, Δt is the discrete time-step, and $n\Delta t$ is large compared to the peak time response of membrane potential. In accord with Robinson et al. (1997),

$$w_j = b^2 j\Delta t e^{-bj\Delta t} \tag{3a}$$

represents the rise and fall of membrane potential in response to input at $t = 0$, incorporating lags due to both synaptic conduction and average dendritic cable delay in a single function. Parameter b regulates both the peak time and mean delay associated with this lag. Time step Δt was set at 0.1 ms, after trials showed that progressive decrements of the time step to 0.01 ms produced only small, asymptotically diminishing effects on the spectral content of the results.

Within unit volumes, both excitatory and inhibitory cell groups are distinguished, each reciprocally and self-coupled, and each coupled at longer range to other unit volumes by cortico-cortical fibres. Delays due to axonal conduction between unit volumes are given by $\Delta\tau = r_{pq}/v$, where $\Delta\tau$ is axonal conduction lag over the distance r_{pq} between the pth unit volume and the qth unit volume and axonal conduction velocity is v.

Coupling strengths are proportional to:

1. The fractional density of synaptic couplings afferent to the dendrites of excitatory and inhibitory cells respectively ($\alpha_{ee}, \beta_{ei}, \mu_{ei}, M_{ee}$, etc as listed in Table 2).
2. The synaptic gains of excitatory and inhibitory synapses, g_e and g_i.
3. Changes in synaptic efficacy, E', representing feedback effects including those of reversal potentials (Kandel and Schwartz 1985). That is, with increasing depolarisation of cell membranes there is an increase in sensitivity to inhibitory synaptic inputs and a decrease in sensitivity to excitatory synapses. These feedback relations are modelled as linear regressions of efficacy with membrane potential

$$\begin{aligned} E'_{ee}(t) &= [1 - V_{e(p)}(t - \Delta t)/V_{eR}], \\ E'_{ei}(t) &= [1 - V_{i(p)}(t - \Delta t)/V_{eR}], \\ E'_{ie}(t) &= [1 - V_{e(p)}(t - \Delta t)/V_{iR}], \\ E'_{ii}(t) &= [1 - V_{i(p)}(t - \Delta t)/V_{iR}] \ , \end{aligned} \tag{4}$$

where the subscripts e and i indicate excitatory and inhibitory potentials, and subscript R a constant-valued reversal potential. Efficacies $\{E'\}$ were applied with smoothing, so that in each case $E(t) = \sum_{j=1}^{n} u_j E'(t - j\Delta t)$, where $u_j = ce^{-cj\Delta t}$, describing an exponential decay of the impact of instantaneous membrane potential upon synaptic efficacy. For high values of c, this decay is rapid, as would be expected for reversal potentials alone.

State equations for the cortical system are then given for the pth unit volume by

$$\begin{aligned} Q_{e(p)} &= \left(1 + e^{a(V_{e(p)} - 3)}\right)^{-1}, \\ Q_{i(p)} &= \left(1 + e^{a(V_{i(p)} - 3)}\right)^{-1} \ , \end{aligned} \tag{5}$$

$$\begin{aligned} V_{e(p)} &= \sum_{j=1}^{n} w_j Q_{ae(p)}(t - j\Delta t), \\ V_{i(p)} &= \sum_{j=1}^{n} w_j Q_{ai(p)}(t - j\Delta t) \ , \end{aligned} \tag{5a}$$

where $Q_{ae(p)}, Q_{ai(p)}$ are afferent synaptic action densities for excitatory and inhibitory cells respectively, in the pth unit volume, receiving local synaptic input at negligible axonal delay and delayed cortico-cortical inputs from qth unit volumes at range r_{pq}, $q = 1 \ldots u$, in accord with

$$\begin{aligned} Q_{ae(p)} = {} & g_e\beta_{ee}E_{ee(p)}Q_{e(p)} - g_i\beta_{ie}E_{ie(p)}Q_{i(p)} \\ & + g_eM_{ee}E_{ee(p)}Q_{s(p)} + g_e\mu_{ee}E_{ee(p)}Q_{ns(p)} \\ & + g_e\sum_{1}^{u}\alpha_{ee}(r_{pq})E_{ee(p)}Q_{e(q)}(t - r_{pq}/v) \ . \end{aligned} \tag{5b}$$

$$\begin{aligned} Q_{ai(p)} = {} & g_e\beta_{ei}E_{ei(p)}Q_{e(p)} - g_i\beta_{ii}E_{ii(p)}Q_{i(p)} \\ & + g_eM_{ei}E_{ei(p)}Q_{s(p)} + g_e\mu_{ei}E_{ei(p)}Q_{ns(p)} \\ & + g_e\sum_{1}^{u}\alpha_{ei}(r_{pq})E_{ei(p)}Q_{e(q)}(t - r_{pq}/v) \ , \end{aligned} \tag{5c}$$

where $\alpha_{ee}(r_{pq})$ and $\alpha_{ei}(r_{pq})$ are partial input synaptic densities, such that $\sum_1^\mu \alpha_{ee}(r_{pq}) = \alpha_{ee}$ and $\sum_1^\mu \alpha_{ei}(r_{pq}) = \alpha_{ei}$. Q_s and Q_{ns} are system inputs. Q_s represents all time-varying components in specific cortical afferents and Q_{ns} is a uniform DC input representing nonspecific cortical activation, which acts as control parameter.

2.2 Standard parameters and definition of units

State variables and parameters, their dimensions and standard values are given in Tables 1 and 2. Where possible, physiologically accurate values have been applied, and certain difficulties of parameterisation have been avoided by the use of normalised units. For details, see Wright (1999).

Table 1. State variables and standard parameters other than synaptic densities. *LFP* Local field potential, *PPD* pulse probability density, *EPSP* excitatory post-synaptic potential, *IPSP* inhibitory post-synaptic potential

V_e	Excitatory LFP	vu
V_i	Inhibitory LFP	vu
Q_e	Excitatory PPD	Dimensionless
Q_i	Inhibitory PPD	Dimensionless
a	Slope parameter	$-\pi/\sqrt{3}$ (vu^{-1})
b	Dendritic time constant	50 s^{-1}
g_e	Excitatory gain	65 vu
g_i	Inhibitory gain	260 vu
c	Decay time constant.	1000 s^{-1}
v	Axonal velocity	9 m/s
$\sqrt{\bar{r}_{pq}^2}$	SD of axonal range	4 mm
V_{eR}	EPSP reversal	12 vu
V_{iR}	IPSP reversal	−0.02 vu
Q_{ns}	Non-specific input	Dimensionless
Q_s	Specific input	Dimensionless

Table 2. Synaptic couplings subscripts ee, ei, etc. indicate synapses between cell types, excitatory to excitatory, excitatory to inhibitory, etc. Types of coupling are: α (cortico-cortical connections), β (intracortical connections), μ (nonspecific cortical afferents) and M (specific afferents). Synaptic density fraction is the proportion of synapses of each type in unit cortical volume. [The exact values used in the simulations are given for completeness (Liley and Wright 1994) although the precision given is greater than is justified from the anatomical data.] Afferent fraction is the proportion of synapses on the excitatory or inhibitory cell dendrites respectively, and are thus the values applied in Eq. (5)

Synaptic coupling	Synaptic density fraction	Afferent fraction
α_{ee}	0.765	0.8693
β_{ee}	0.0845	0.0960
β_{ei}	0.0149	0.1242
α_{ei}	0.100	0.8333
β_{ie}	0.0228	0.0259
β_{ii}	0.004	0.0333
μ_{ee}	0.0077	0.0088
μ_{ei}	0.0011	0.0092
$M_{ee,i}$	Not given	

2.3 Configuration of simulation

An extended area of the cortex was simulated by unit volumes in a 20×20 matrix, each volume connected with its neighbours so that the coupling strengths, $\alpha_{ee}(r_{pq})$ declined with r_{pq} as a Gaussian function with standard deviation of four distance units, where a distance unit is the side of one cell of the 20×20 matrix. This approximates to distribution of cortico-cortical fibres in the cat brain if the distance unit is taken as about 0.9 mm. Boundary conditions were toroidal in all simulations reported. The application of absorbing boundary conditions and changes in matrix size were also studied and these changes did not affect the results to be reported.

2.4 Added assumptions

For the results which follow, two further assumptions proved necessary. Discussion of these assumptions is reserved to Sect. 4:

1. A single object moving in the sensory field stimulates feature detectors in primary sensory neurones so that, over any short epoch, afferent volleys in the sensory pathway are correlated at zero lag – i.e. inputs from a single stimulus object give rise to spatially coherent input at the cortical level. Distinct stimulus objects are thus uncorrelated with each other by definition.
2. Cortical signal-to-noise ratio rises with cortical activation – i.e. the spatially coherent component of inputs from stimulus objects is greater relative to background noise at higher levels of cortical activation.

2.5 Simulation inputs and outputs

Two configurations were used in these studies.

2.5.1 Stationary driving inputs. These simulations follow Wright (1997), Robinson et al. (1998), and Chapman et al. (in press) and are here used to succinctly demonstrate the basic physical mechanism by which synchronous oscillation appears in the simulation, as a prelude to the moving-bar studies.

Specific inputs, Q_s, imitated time-variation of a complex localised input to selective sites in the cortex. These were delivered as two independent (asynchronous) time series of zero-mean white noise (Marsaglia and Zaman 1987) of small amplitude, input to the unit volumes situated at sites in one row of the matrix of elements, and separated by five intervening elements. Input was received at both excitatory and inhibitory cell dendritic junctions of the driven sites.

Non-specific inputs, Q_{ns}, imitated the action of reticular, catecholaminergic and other diffuse inputs to cortex, and were delivered uniformly to all unit volumes in the matrix as constant non-zero inputs, throughout the duration of each simulation run.

Although both types of input are extremely simple compared to real cortical input, results are sufficiently general for interpretation of results from inputs of greater complexity, as will be discussed.

Outputs were recorded as $V_e(t)$ and $Q_e(t)$ from all other elements in the field, and were used to calculate lagged cross-correlations, and to calculate the major principle components (spatial eigenmodes) of activity in the simulated cortical field, after prior removal of the signals from the Q_s-driven sites. Spatial eigenmodes were calculated using spatial principal component analysis (PCA) (Preisendorfer 1988) to resolve the wave activity generated in the simulation into equivalent modes of spatially stationary synchronous activity.

Simulation runs began with $\{Q_e, Q_i\}$ all initially zero, and ran for 1 s, which ensured steady-state (signal mean stationary) conditions were achieved. Outputs were analysed over the subsequent second, to obtain data for cross-correlations, and 2 s to obtain data for principal component analysis – the results of both these measures differing negligibly with further prolongation of the run time.

2.5.2 Moving bars. The simulation of moving bars implicitly defines a single moving object as a set of cross-correlated inputs, more or less spatially contiguous.

The simulated bars, which are Q_s inputs, moved across the simulated cortical surface, while non-specific activation, Q_{ns} was delivered uniformly as before. In some experiments the Q_{ns} inputs included spatiotemporal white noise in addition to the usual DC component, as will be reported. This diffuse noise was provided by input of white noise time series initiated from different seed values to each element in the cortical matrix, allowing a more realistic representation of cortical activation. The rms amplitude of specific inputs was 0.01 units, and the point amplitude of diffuse field noise is reported in Sect. 3 in the same units.

Moving bars were orientated along the rows of the matrix, and moved up or down the columns. The standard apparent velocity of movement of the simulated cortical surface was 24.4 mm/s, so that a complete single sweep of the bars occurred in 0.8192 s. Results from these runs required ensemble averaging to yield sufficient confidence on magnitude, although robust synchrony was apparent in individual sweeps. Bar speed was varied in control experiments.

Short bars, of 3 mm length in cortical projection, and a long bar of 20 mm (the width of the matrix) were simulated, each with an apparent width of 1 mm (one cortical element). The long bar thus reached completely across the simulated cortical surface, while the short bars were aligned so as to pass close to the two reference sites subsequently used for cross-correlation. Usually bar movements were such that the reference sites were crossed simultaneously by the two short bars, or by the length of the long bar, whatever the direction of movement. This occurred when the reference sites were in the tenth row of the matrix. A control condition was the case in which the reference sites were located in the fifth row of the matrix – that is, as far as possible from the zeroth and tenth rows of the matrix, the two positions where oppositely moving bars pass each other. This exceptional condition we called the "remote passing" condition, to contrast it to the more general "proximal passing" condition.

In the experiments to be reported, the two short bars moved so as to straddle both reference sites, without directly driving either. This is not critical to the results obtained, and it is relevant only that the short bars pass close to the reference sites.

To prevent stepping discontinuities, the forward movement of the bars was smoothed in imitation of a 1-mm-wide bar moving continuously.

In both long and short bars, only every second element along the length of the bar was driven, with a 50% probability of receiving input at each time step. In no case did the reference sites themselves receive direct specific (Q_s) inputs, as to do so confounds cross-correlations to be made with regard to field effects in the simulation with the direct content of the inputs. Both zero-mean and non-zero mean Q_s inputs were applied in different simulation runs.

Finally, the white noise time series used to drive any single bar were arranged according to either of two conditions. In the "synchronous bar" condition, all inputs to a single bar were synchronous (identical), while they were asynchronous (uncorrelated) between separate bars. This condition meets the definition of a single moving object, as mentioned above. In the "asynchronous bar" condition, all inputs within, as well as between bars, were uncorrelated.

3 Results

3.1 Stationary driving inputs

Figure 1 shows the essential mechanism whereby synchronous oscillation arises in these simulations, as reported in Wright (1997), Robinson et al. (1998), and Chapman et al. (in press). We wish to emphasise that zero-lag synchrony is a universal attribute of continuum fields or neural networks which have summing junctions with delay (dendrites) and couplings (axons) with transmission delay which is small compared to dendritic delay. Synchrony then occurs by summation of even (in phase) components in the separated input signals, and cancellation of odd (out of phase) components. This effect does not require non-linearity.

When twin uncorrelated signals are delivered to the cortical surface, a pattern of zero-lag synchrony develops around the driving sites, as is shown in the upper diagrams in Fig. 1. Similar results can be obtained for cross-correlations of any reference point close to either of the sites of white noise input. The pattern of zero-lag synchrony has been shown to be sensitive to inhomogeneities in the strength of connections between elements of the matrix, whether these reflect structural or dynamic coupling gains. Conversely, uniform multiplications of the connection strength throughout the field have no effect on the pattern of synchrony. Similarly, uniform increases in cortical activation (Q_{ns}) have little effect, so long as the level of activation remains below a critical level at which limit cycles develop. A highly non-linear dynamic emerges at very high Q_{ns} and this condition was avoided throughout the current studies.

The middle diagrams in Fig. 1 show the first and second eigenmodes revealed by PCA. The first eigenmode is similar in form to the field of zero-lag maximum cross-correlation, and consumes the majority of the variance in the field. It can be shown (Chapman et al., in press) that the first eigenmode follows even (in-phase) transients in the driving inputs and the second eigenmode follows odd (anti-phase) transients in the same inputs. The lower diagrams of Fig. 1 show schematically the way in which the summation of even components in the surrounding field creates the first eigenmode, which predominates over the second eigenmode – the form of the second mode being attributable in part to cancellation of the odd signals spreading into the field from the inputs. Predominance of the first mode is greatest in the field near the driving sites – hence the field of zero-lag synchrony.

3.2 Impact of concurrent noise and cortical activation – static case

Figure 2 shows the cross-correlations found between two sites within the field of zero-lag synchrony generated by the two stationary sites of driving with asynchronous noise, while the rms amplitude of input to the driving sites was held constant and diffuse noise throughout the field was increased.

With increasing field noise, the cross-correlation decreases as expected, but there is little effect on the cross-correlations obtained when the degree of cortical activation is changed fourfold. The lack of sensitivity of cross-correlation to Q_{ns} alone is accounted for by the fact that the first and second eigenmodes of field activity increase concurrently in amplitude in response to the

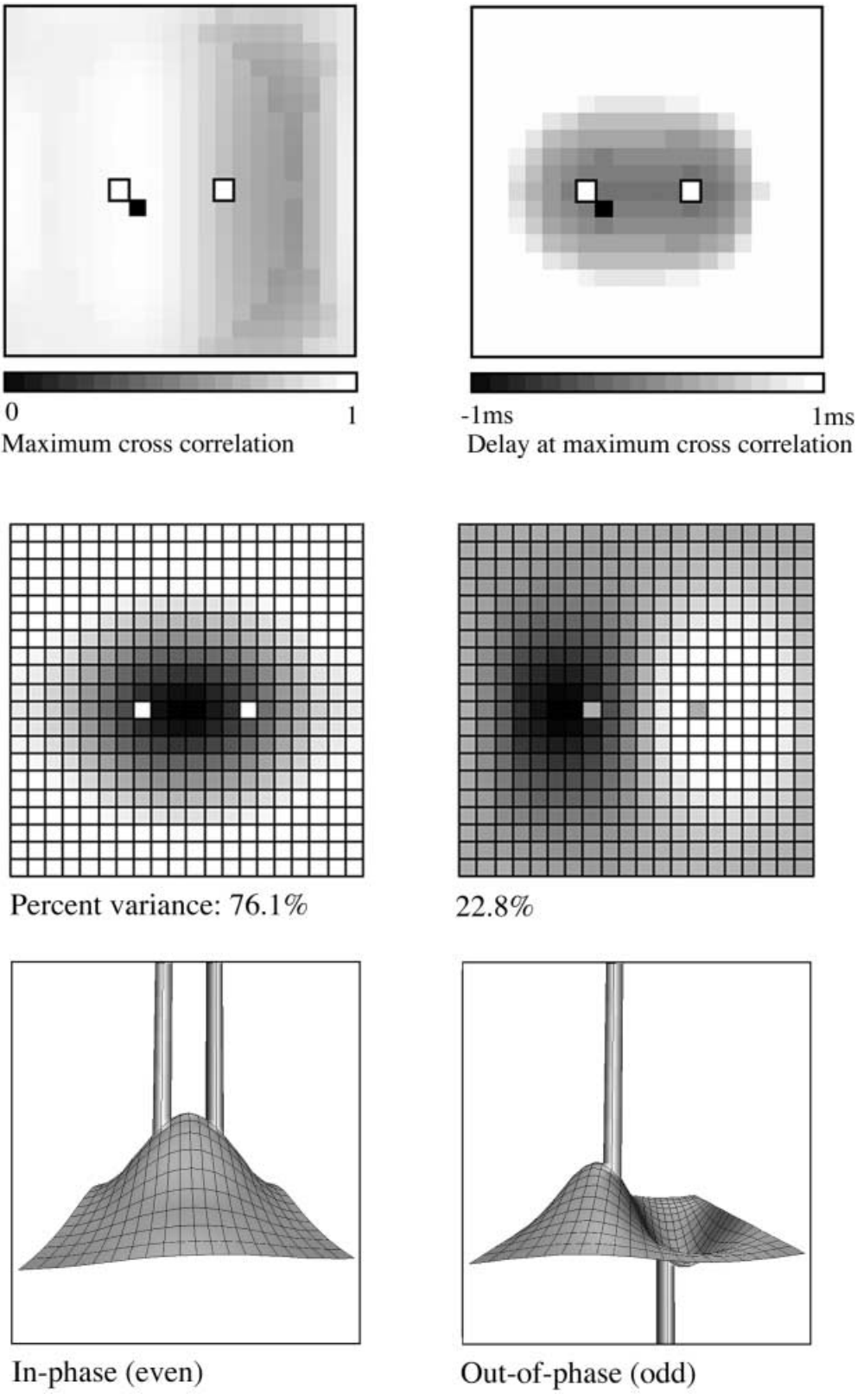

Fig. 1. Essential properties of synchronous oscillation. *Top figures* A representation of the simulated cortical surface. *Open squares* represent the sites of input of uncorrelated white noise. The *filled square* is the reference point from which cross-correlations are calculated with respect to the rest of the field. *Top left* Maximum positive cross-correlations. *Top right* Delay associated with maximum cross-correlation. *Middle figures* The first and second principal eigenmodes of activity on the simulated cortical surface, obtained from the same data used to generate the top figures. *Bottom figures* Schematic "freeze frame" images of potentials (or pulse densities) on the simulated cortical surface seen when the twin inputs are sine waves, of any single frequency. *Bottom left* Potentials in the field when the sine waves are in phase. *Bottom right* Potentials in the field when the sine waves are of reverse phase

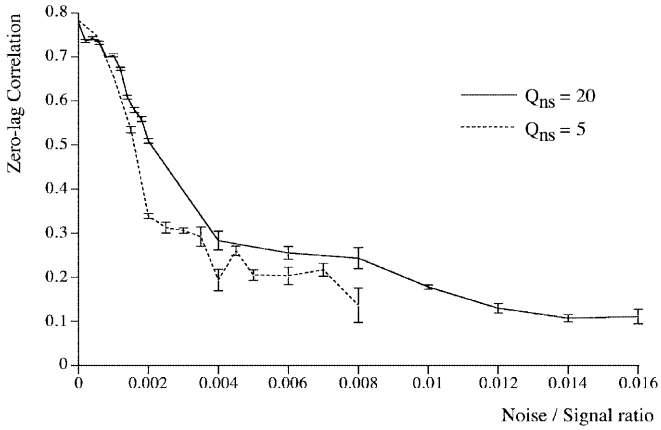

Fig. 2. Dependency of cross-correlation on signal/noise ratio and independence from uniform cortical activation in the absence of overlying noise. Zero-lag cross-correlation obtained between the reference site shown in Fig. 1, and another site located at the point of mirror-image symmetry, adjacent to the right hand input site. Mean and SEM of cross-correlations from 20 1-s simulation runs. In addition to the twin sites of asynchronous noise input to the same driving sites as in Fig. 1, spatiotemporally white noise has been input to all other sites in the field. The noise-to-signal ratio refers to the ratio of rms amplitude of the random field noise, to that at the twin "driving" sites. Results are shown for two widely different conditions of non-specific cortical activation, as indicated by the value of parameter Q_{ns}

uniformly increasing dynamic gain (dQ/dV), produced by increase in Q_{ns}. Such small increase in cross-correlation as occur with increasing Q_{ns}, is manifest at higher "noise-to-signal" ratios.

3.3 Moving bars

Figure 3a shows the simulation's reproduction of the findings of Gray et al. (1989) and Eckhorn et al. (1988) for moving bars. It can be seen that LFP time series, power spectra, and cross-correlations closely approximate experimental findings. Only a single-sweep LFP time series is shown here, but superposition of LFP from repeated sweeps shows that they are not phase-locked to the presentation of the stimulus, in the same manner as noted experimentally by Eckhorn et al. (1988). The particular frequency content of the LFP time series, which matches the predominance of power in the gamma range typically seen in experiments, is a consequence of the choice of Q_{ns} applied in these particular simulations. At much lower values of Q_{ns}, the spectral content resembles the EEG at lower levels of activation – yet the cross-correlation values are little affected.

Notably, the highest zero-lag cross-correlation is seen for the single large bar, next for two short bars moving in the same direction, and lowest for the two short bars moving in opposite directions. The relative magnitude of these cross-correlations is essentially independent of Q_{ns}.

Figure 3b shows data from simulations similar to those shown in Fig. 3a, except that the "asynchronous bar" condition has been applied. Notably, the long bar now yields no higher cross-correlation than two bars moving in the same direction.

Figure 3c uses conditions matched to those in Fig. 3b, and cross-correlations are shown for both the standard "proximate passing" and the "remote passing" conditions. Variation in the situation of the reference sites relative to the position of passing has little effect on the degree of cross-correlation, so long as the sites remain in a symmetric relation to the tracks of passage of the bars.

In all permutations of the various conditions applied, we found that when the diffuse field noise was zero, no differences could be demonstrated in cross-correlation for two bars moving in the same, versus opposite, directions. This result may appear paradoxical, since the two bars moving together are always closer to each other, therefore interact more strongly, and create larger amplitude travelling waves in the medium. However, this greater wave amplitude does not lead to any significant difference in the partition of energy between the first and second eigenmodes of the waves. Thus, cross-correlations (which normalise absolute magnitude) are not sensitive to the relative direction of bar movement so long as the paths travelled are otherwise identical.

The introduction of diffuse field noise produces sensitivity to the relative direction of movement of the bars, as shown in Fig. 3d. This result is accounted for as follows: when the two bars move in the same direction, the absolute magnitude of both the first and second eigenmodes is enhanced, although their relative magnitudes are unchanged. With equivalent levels of additive field noise, the signal/noise ratio, which is measured by cross-correlation, is then higher for the case in which the bars move together, and lower when they move in opposite directions.

3.4 Effect of cortical activation with concurrent increase in cortical signal-to-noise ratio – two moving bars

Figure 4 shows that, so long as constant amplitude diffuse spatio-temporal noise is applied to the field, then the zero-lag synchrony increases as cortical activation is increased. These results are closely similar to the experimental results reported in Munk et al. (1996).

3.5 Consequences of other alterations of signal properties

Qualitatively, the results in Figs. 3 and 4 do not depend upon the input signals associated with the moving bar having a non-zero mean. The results shown are for zero-mean input signals. Non-zero mean of the moving-bar inputs inevitably adds to the cross-correlation observed, unless high-pass filtering is applied to the output signals before cross-correlation is performed. (This offset or envelope effect is often removed experimentally by the use of high pass filters to allow for envelope of the input signal.) No input signal correlations are required for synchrony to emerge, no matter what the size or direction of movement of the bars.

The results shown are also independent of the choice of bar speed, which was doubled and halved from the standard speed without significant consequence on the

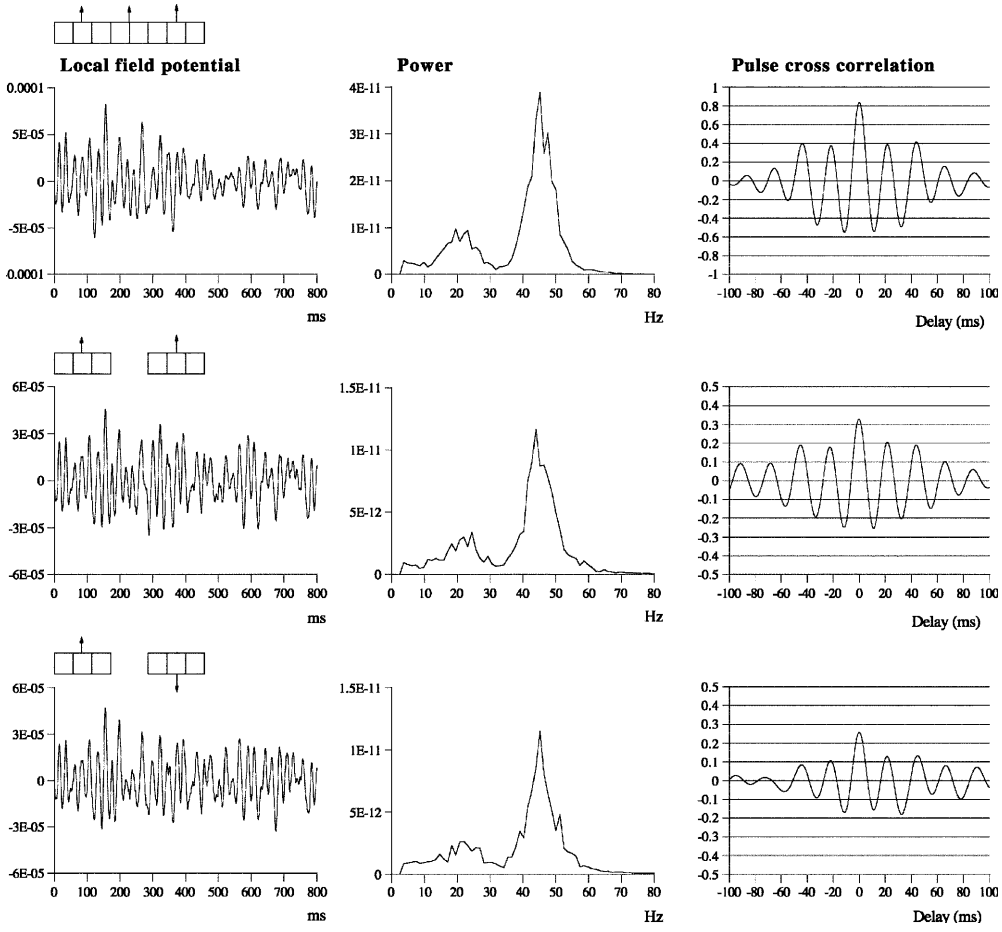

Fig. 3a. Effects of stimulus extension and coherence on synchronous oscillation. Oscillations of local field potential (*left-hand figures*), spectral power (*middle figures*) and pulse-density cross-correlations (*right-hand figures*) in the simulated cortical field, as zero-mean inputs are swept across the field in imitation of the visual stimuli associated with moving bars. A single bar has coherent white noise inputs applied at each portion of the bar. Separate bars have no input signal correlations – see text for details. Diffuse field noise amplitude 0.000033. *Top graphs* Two short bars moving in the same direction. *Middle graphs* Two short bars moving in opposite directions. *Bottom graphs* One long bar moving across the field. In this figure and in all following figures, cross-correlations were associated with standard errors of approximately 0.005 ± 0.001. Thus, visible differences in cross-correlation are highly statistically significant

results. This is not congruent with the finding of Eckhorn et al. (1988) that increasing stimulus speed was associated with gamma-band oscillation at increasing frequency, and implies that such a relation would require stimulus speed to be associated with the level of cortical activation.

With regard to Fig. 4, if the amplitude of the specific stimuli does not increase with cortical activation, or if there is no diffuse field noise, then the maximum cross-correlation does not alter significantly.

4 Conclusions

The above results appear to capture concurrently the physiologically observed cross-correlation results of moving-bar experiments and influences of reticular formation stimulation, along with realistic representation of LFP spectral power, and absence of phase-locking of response to the input signal.

The simulated cortical medium has the capacity to selectively eliminate odd components in the asynchronous input signals. This basic property carries over into more complex moving stimuli, is little effected by the level of cortical activation and, correspondingly, does not require oscillation in the gamma range for synchrony to occur.

The ubiquity of synchrony without dependence upon any correlation in the inputs does not provide a sufficient explanation for either the experimental differences dependent on the direction of bar movement, or the effects of cortical activation upon synchrony. Reproduction of these physiological results depends upon two additional assumptions – firstly, that a single stimulus object can be defined as a spatially coherent set of inputs, and secondly that the signal-to-noise ratio of inputs increases concurrently with cortical activation.

In the results reported above, the first assumption proved necessary only to account for the enhanced magnitude of cross-correlations found when the stimulus is a long single bar, rather than two short bars moving in the same direction. This is a robust finding, both physiologically and within our simulations.

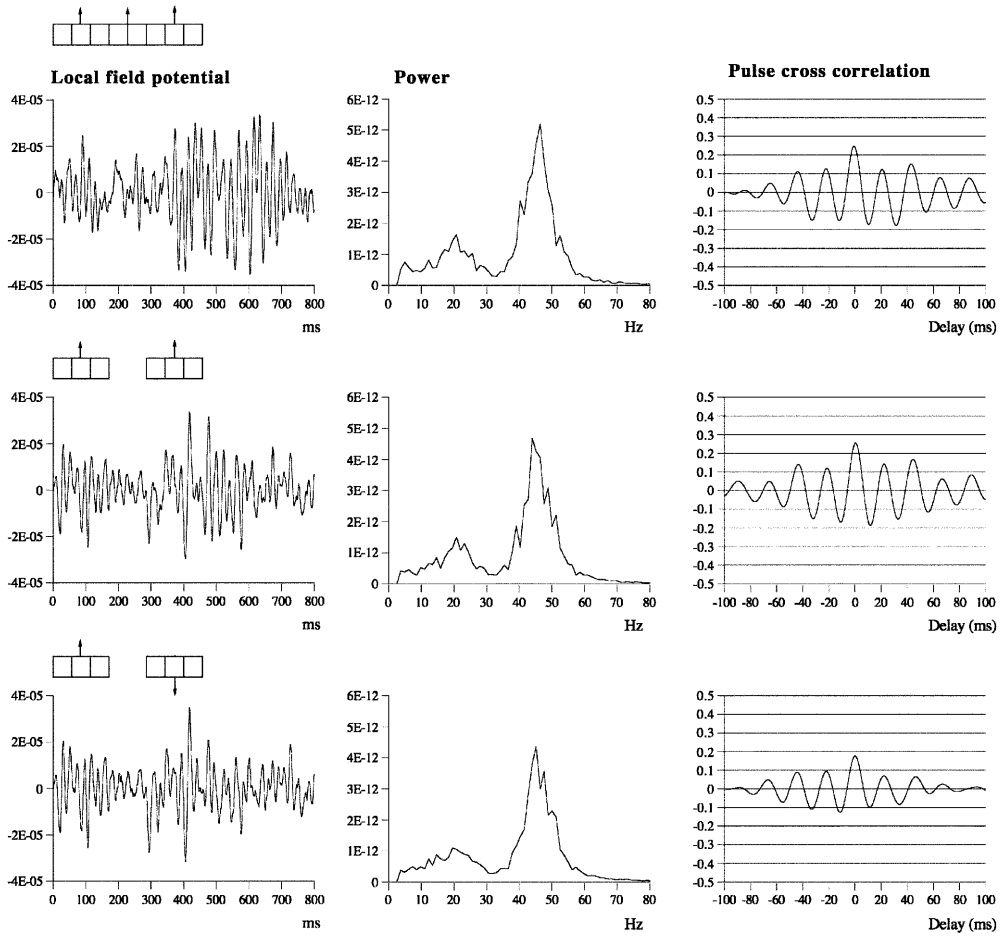

Fig. 3b. Results shown are derived as for **3a** except that uncorrelated white noise was delivered to all parts of each bar, as well as being uncorrelated between bars. Diffuse field noise amplitude 0.000025

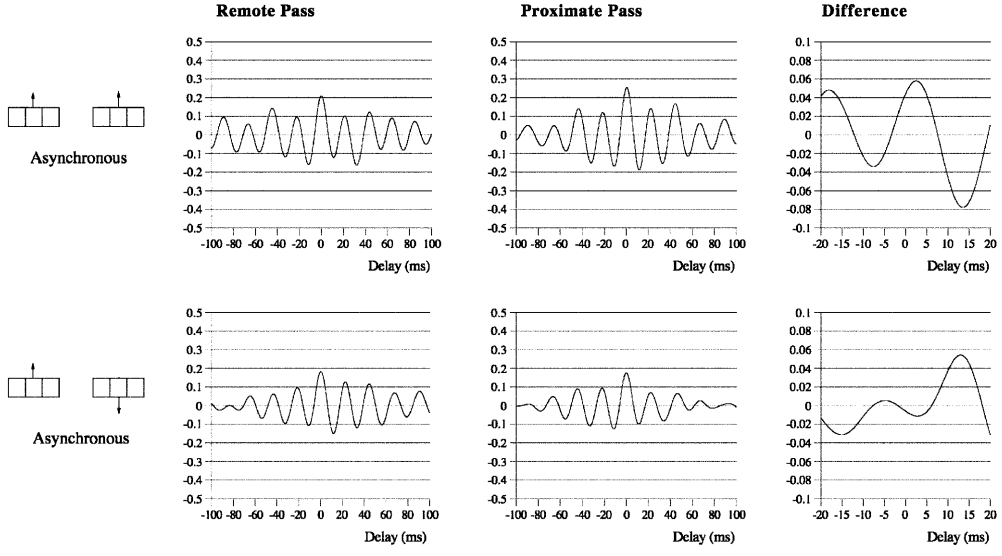

Fig. 3c. Cross-correlations for the asynchronous bar case, with diffuse field noise 0.000025, for bars moving in the same and opposite directions. Reference points at the matrix row at which the oppositely moving bars pass each other (proximate pass) or in the same columns but remote from the passing row (remote pass). See text for details. Differences are between the remote and proximate conditions. The small differences remain statistically significant

The first assumption may be usefully regarded as providing a definition of a stimulus object. Extension of this definition leads to the notion that any spatially synchronous pattern of activity in the brain is an "object" – either the representation of a physical object via sensory input, or a coherent pattern partly internally generated, and thus a representation of a mental object. This is equivalent to von der Malsburg's (1983) original proposition that synchronous oscillation is the means by which binding is mediated. Concurrent stimulation of receptor cells in the cortex or elsewhere must produce synchrony in the afferent bombardment over at least some frequencies, as has been remarked in physiological experiments (e.g. Kreiter and Singer 1996; Neuenschwander and Singer 1996; Steriade et al. 1996) and demonstrated in models of the visual pathways (Ghose

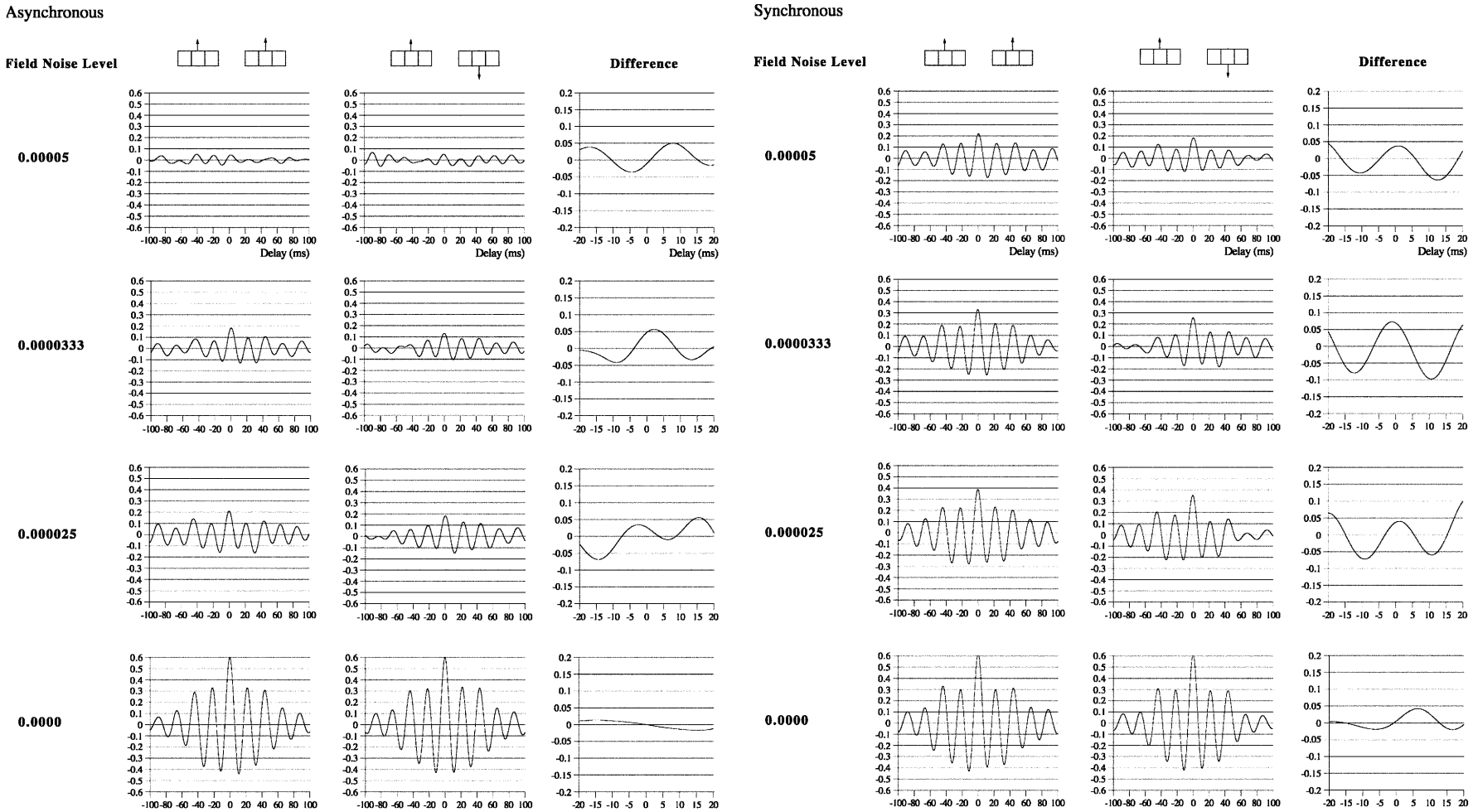

Fig. 3d. Cross-correlations from proximate-pass reference sites with differing levels of diffuse field noise, for both asynchronous and synchronous bar conditions. Differences are with respect to the directions of bar movement shown in the graphs to the left of each difference graph. The difference produced by direction of movement is zero at zero lag in the absence of diffuse field noise

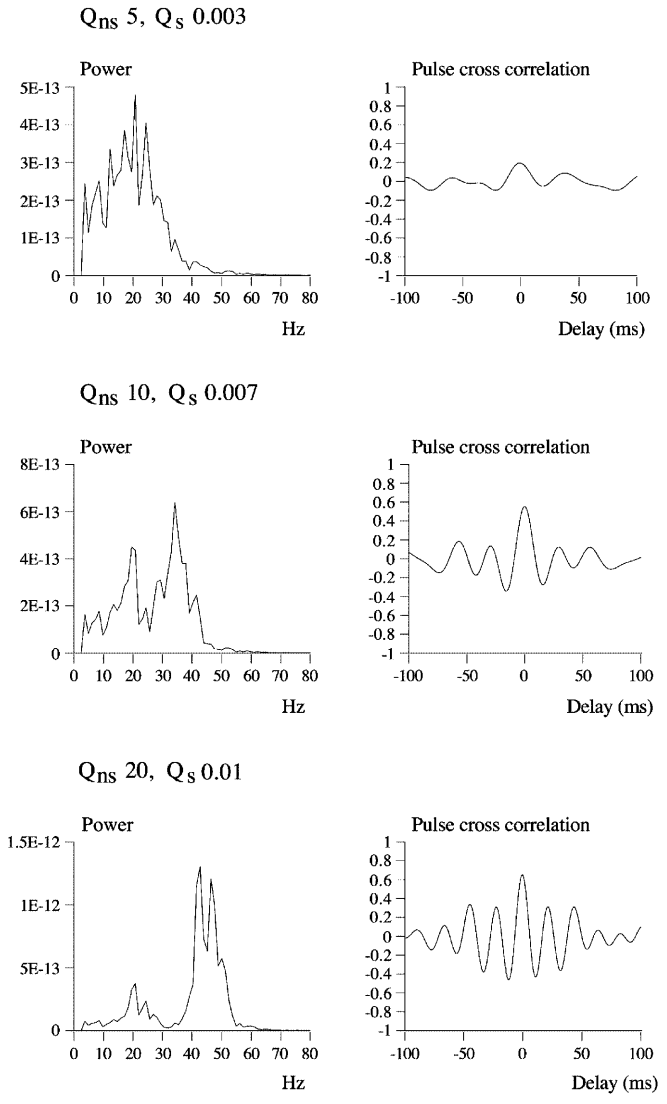

Fig. 4. Effects of cortical activation on synchronous oscillation in the presence of uniform field noise. Average power spectra and pulse-cross-correlations calculated as for the two short bars moving in the same direction case (Fig. 3a). Here, uniform amplitude spatio-temporally white noise was applied throughout the field, and both the level of cortical activation (Q_{ns}) and the amplitude of the signals associated with the moving bars (Q_s) were raised concurrently

and Freeman 1997). It is not necessary that coherence in the afferent volleys be complete at all frequencies to give rise to the effects reported.

The second assumption we have shown to account for experimentally observed increases in cross-correlation with increasing cortical activation. More generally, a degree of diffuse field noise seems essential to account for the sensitivity of cross-correlation to relative direction of movement of multiple bars. There are implications here for the coherent infomax hypothesis, regarding synaptic modification and learning in relation to synchronous oscillation (Phillips and Singer 1997). The information-theoretical derivation of coherent infomax leaves unexplained how information from different stimulus configurations becomes selectively distributed over synapses. Our findings suggest that noise may be required to enhance contrasts of relative synaptic activation when stimulus objects move in relation to each other in different ways.

A relation between cortical activation and signal/noise ratio is without general proof from physiological data. It is inherently plausible, since cortical activation is associated with enhanced cortical information processing. It is loosely supported by the close association of pulse and LFP in cortical activity in the gamma band, as opposed to the notoriously low associations of EEG and pulse activity at lower EEG frequencies and cortical activation (Stryker 1989). A part of the enhancement of signal versus noise may be attributed to a further property of synchronous oscillation which is only weakly apparent in these simulations. As shown in Fig. 2, increasing cortical activation does somewhat enhance cross-correlation at medium ranges of signal-to-noise. This effect would be further enhanced were the effects of cortical depth or repeated passage of signals through layers of relay cells such as the cell layers of the lateral geniculate body included.

We were forced to make these assumptions because of the simplicity of representation of the input pathways in our model. The model of Lumer et al. (1997a,b), in contrast, dealt in detail with the input pathways, and reproduced synchronous oscillation as a general property of jitter stimuli introduced to their neural networks. Similar considerations hold for the earlier cited works on feedforward modelling (Schillen and Konig 1994; Fuentes et al. 1996; Xing and Gerstein 1996; Juergens and Eckhorn 1997). It would appear that these approachs and ours may be complementary.

One property of experimental synchronous oscillation which has not been reproduced is the relation of bar speed to the LFP spectral content (Eckhorn et al. 1988). Within the present model, this could be explained by the further assumption that faster moving stimuli contribute more strongly to cortical activation, whether directly or via collaterals in the reticular-activating system. This would have the effect of shifting the LFP spectrum further to the right, in accord with the experimental observation. In a study of somatic sensory synchrony by Ruiz et al. (1995), faster stimuli were associated with increased cell-firing rates, consistent with an association between stimulus velocity and total activation.

The present results do not include two further factors which may be crucial to quantitative reproduction of synchronous oscillation, whereas we have been able to obtain only the correct relative changes in cross-correlation magnitude according to different experimental conditions.

Firstly, we have here considered only symmetrical cortical couplings and uniform cortical activation whereas, in reality, both these factors are inhomogeneous, and systematically so. This may explain why our simulations did not capture the extremes of cross-correlation seen experimentally, in which cross-correlation may be sometimes reduced to zero for bars moving in opposite directions, while quite high correlations are seen for movements in the same direction. As earlier remarked, there is other evidence in similar simulations

that non-uniform structural and dynamic coupling strengths change the patterns of synchronisation for static inputs. Introduction of non-uniform couplings would open the possibility of detailed simulation of synchrony – for example, between cortical sites of similar orientation preference – since such sites are more strongly coupled than sites of dissimilar orientation preference (Malach et al. 1993; Yoshioka et al. 1996). Like-to-like connectivity might also hold for velocity characteristics of stimuli, as is predicted by certain Hebbian models for the development of intracortical intrinsic connections (Alexander et al., in preparation).

Secondly, these results do not allow for the possible occurrence of non-linear phase locking as a mechanism of synchronous oscillation. At higher levels of cortical activation, non-linear phase locking occurs in these simulations, as reported in Chapman et al. (in press). This additional mechanism opens the door to modelling of the putative role of synchrony in image segmentation, as shown in abstract simulations by Wang (1996). The form of synchronisation modelled here acts as a means of rapid synchronisation of cortical areas active for whatever reason, i.e. the present mechanism would appear sufficient to mediate binding.

Beyond these considerations of intracortical dynamics and input path properties, still more complete accounts of synchronous oscillation will likely require an account of cortical/subcortical interactions, processes which appear required to organise the binding and uncoupling of cortical assemblies during ongoing perception and cognition (Miltner et al. 1999; Rodriguez et al. 1999).

Thus, extensions of these experiments may be expected to enable testing of the mechanisms proposed against increasingly complicated physiological experiments – at the price that experimentally, concurrent levels of cortical activation and the detailed local connectivity of cells must be explicitly considered.

References

Abarbanel H, Rabinovich M, Selverston A, Bazhenov M, Huerta R, Sushchik M (1996) Synchronization in neural networks. Physics-Uspekhi 39: 337–362

Alexander DM, Bourke PD, Sheridan P, Konstandatos O, Wright JJ Emergence under Hebbian learning of local maps in the primary visual cortex: orientation preference in the tree shrew. (in preparation)

Amit DJ (1998) Simulation in neurobiology: theory or experiment? Trends Neurosci 21: 231–237

Bressler SL, Coppola R, Nakamura R (1993) Episodic multiregional cortical coherence at multiple frequencies during visual task performance. Nature 366: 153–156

Chapman CL, Bourke PD, Wright JJ (in press) Spatial eigenmodes and synchronous oscillation: coincidence detection in simulated cerebral cortex. J Math Biol

Eckhorn R, Bauer R, Jordon W, Brosch M, Kruse W, Munk M, Reitboeck HJ (1988) Coherent oscillations: a mechanism of feature linking in the visual cortex? Biol Cybern 60: 121–130

Fuentes U, Ritz R, Gerstner W, Van Hemmen JL (1996) Vertical signal flow and oscillations in a three layer model of the cortex. J Comp Neurosci 3: 125–136

Ghose GM, Freeman RD (1997) Intracortical connections are not required for oscillatory activity in the visual cortex. Vis Neurosci 14: 963R–979R

Gray CM, Singer W (1989) Stimulus-specific neuronal oscillations in orientation columns of cat visual cortex. Proc Natl Acad Sci USA 86: 1698–1702

Gray CM, Konig P, Engel AK, Singer W (1989) Oscillatory responses in cat visual cortex exhibit intercolumnar synchronisation which reflects global stimulus properties. Nature 388: 334–337

Juergens E, Eckhorn R (1997) Parallel processing by a homogeneous group of coupled model neurones can enhance, reduce and generate signal correlations. Biol Cybern 76: 217–227

Kandel ER, Schwartz JH (1985) Principles of neural science 2nd edn. Elsevier, New York, pp 111, 113–115

Kreiter AK, Singer W (1996) Stimulus-dependent synchronisation of neuronal responses in the visual cortex of the awake macaque monkey. J Neurosci 16: 2381–2396

Liley DTJ, Wright JJ (1994) Intracortical connectivity of pyramidal and stellate cells: estimates of synaptic densities and coupling symmetry. Network 5: 175–189

Livingstone MS (1996) Oscillatory firing and interneuronal correlations in squirrel monkey striate cortex. J Neurophysiol 75: 2467–2485

Lumer ED, Edelman GM, Tononi G (1997a) Neural dynamics in a model of the thalamocortical system. I. Layers, loops, and the emergence of fast synchronous rhythms. Cerebral Cortex 7: 207–227

Lumer ED, Edelman GM, Tononi G (1997b) Neural dynamics in a model of the thalamocortical system. II. The role of neural synchrony tested through perturbations of spike timing. Cerebral Cortex 7: 228–236

Malach R, Amir Y, Harel M, Grinvald A (1993) Relationship between intrinsic connections and functional architecture revealed by optical imaging and in vivo targeted biocytin injections in primate striate cortex. Proc Natl Acad Sci USA 90: 10469–10473

Malsburg C von der (1983) How are nervous structures organised? In: Basar E, Flohr H, Haken H, Mandell AJ (eds) Synergetics of the brain. Springer, Berlin Heidelberg New York

Marsaglia G, Zaman A (1987) Towards a universal random number generator. Florida State University Report: FSU-SCRI-87-50

Miltner WH, Braun C, Arnold M, Witte H, Taube E (1999) Coherence of gamma-band EEG activity as a basis for associative learning. Nature 397: 434–436

Munk MHJ, Roelfsema PR, Konig P, Engel AK, Singer W (1996) Role of reticular activation in the modulation of intracortical synchronisation. Science 272: 271–273

Neuenschwander S, Singer W (1996) Long range synchronisation of oscillatory light responses in the cat retina and lateral geniculate nucleus. Nature 379: 728–733

Palm G, Wennekers T (1997) Synchronicity and its use in the brain. Behav Brain Sci 20: 695–696

Phillips WA, Singer W (1997) In search of common foundations for cortical computation. Behav Brain Sci 20: 657–722

Preisendorfer R (1988) Principal component analysis in meteorology and oceanography. Elsevier, New York

Robinson PA, Rennie CJ, Wright JJ (1997) Propagation and stability of waves of electrical activity in the cerebral cortex. Phys Rev E 55: 826–840

Robinson PA, Wright JJ, Rennie CJ (1998) Synchronous oscillations in the cerebral cortex. Phys Rev E 57: 4578–4588

Rodriguez E, George N, Lachaux JP, Martinerie J, Renault B, Varela FJ (1999) Perception's shadow: long-distance synchronisation of human brain activity. Nature 397: 430–433

Ruiz S, Crespo P, Romo R (1995) Representation of moving tactile stimuli in the somatic sensory cortex of awake monkeys. J Neurophysiol 73: 525–537

Schillen TB, Konig P (1994) Binding by temporal structure in multiple feature domains of an oscillatory neuronal network. Biol Cybern 70: 397–405

Segev I (1995) Dendritic processing. In: Arbib MA (ed) The handbook of brain theory and neural networks part III. MIT Press, Cambridge, Mass., pp 282–289

Singer W (1994) Putative functions of temporal correlations in neocortical processing. In: Koch C, Davis JL (eds) Large scale neuronal theories of the brain. MIT Press, Cambridge Mass., pp 201–237

Singer W, Gray CM (1995) Visual feature integration and the temporal correlation hypothesis. Annu Rev Neurosci 18: 555–586

Steriade M, Amzica F, Contreras D (1996) Synchronisation of fast (30–40 Hz) spontaneous cortical rhythms during brain activation. J Neurosci 16: 392–417

Stryker MP (1989) Is grandmother an oscillation? Nature 388: 297–298

Thomson AM (1997) Activity dependent properties of synaptic transmission at two classes of connections made by rat neocortical pyramidal neurons in vivo. J Physiol (Lond) 502: 131–147

Thomson AM, West DC, Hahn J, Deuchars J (1996) Single axon IPSP's elicited in pyramidal cells by three classes of interneurones in slices of rat neocortex. J Physiol (Lond) 496: 81–102

Wang D (1996) Object selection based on oscillatory correlation. Technical report 67. Department of Computer and Information Science and Center for Cognitive Science, The Ohio State University, Columbus, Ohio

Wennekers T, Palm G (1997) On the relation between neural modelling and experimental neuroscience. Theor Biosci 116: 267–283

Wilson MA, Bowers JM (1991) A computer simulation of oscillatory behaviour in primary visual cortex. Neural Comput 3: 498–509

Wright JJ (1997) EEG simulation: variation of spectral envelope, pulse synchrony and approx. 40Hz oscillation. Biol Cybern 76: 181–194

Wright JJ (1999) Simulation of EEG: dynamic changes in synaptic efficacy, cerebral rhythms, and dissipative and generative activity in cortex. Biol Cybern 81: 131–147

Xing J, Gerstein GL (1996) Networks with lateral connectivity. I. Dynamic properties mediated by the balance of intrinsic excitation and inhibition. II. Development of neuronal grouping and corresponding receptive field changes. III. Plasticity and reorganisation of somatosensory cortex. J Neurophysiol 75: 184–232

Yoshioka T, Blasdel GG, Levitt JB, Lund JS (1996) Relations between patterns of intrinsic lateral connectivity, ocular dominance, and cytochrome oxidase-reactive regions in macaque monkey striate cortex. Cerebral Cortex 6: 297–310